Comparison between two approaches to simulate the mass loss in cavitation erosion

Thierry Choffat, Regiane . Fortes Patella, Stéphane Barre

Sixth International Symposium on Cavitation
CAV2006, Wageningen, The Netherlands, September 2006

COMPARISON BETWEEN TWO APPROACHES TO SIMULATE THE MASS LOSS IN CAVITATION EROSION

Thierry CHOFFAT - LEGI – INP Grenoble, France : thierry.choffat@hmg.inpg.fr
Regiane FORTES PATELLA - LEGI – INPG, France
Stéphane BARRE - LEGI – INPG, France

ABSTRACT

To carry on with physical approaches and numerical simulations proposed in previous works [Fortes, 1998a, 1998b, 2000, 2001] [Choffat 2003], a simulation tool has been performed in order to evaluate, from pitting tests, the erosion (mass loss) of materials exposed to cavitating flows.

The numerical tool applies models proposed by [Karimi, 1987] and [Reboud, 2001]. The first model consists in a static one-dimensional approach based on work-hardening of the materials. The second implemented model includes fatigue criterion and represents a dynamic 2D axisymmetric approach.

The code simulates, from a given pit distribution obtained by experimental tests, cavitation impacts on the solid samples and predicts material damage. Based on experimental data supplied by EdF-R&D (Electricité de France), a first application example of the models was carried out in order to illustrate the procedure and compare models. A qualitative analysis was done and an influence study of simulation parameters on quantitative results are in progress to better evaluate physical approaches. More experimental results concerning metallurgical and dynamic solid characterization, as well as coupled cavitation mark and erosion tests are required in order to validate and calibrate proposed models.

INTRODUCTION

In order to predict the erosion of a material exposed to a cavitating flow and thus optimise devices, simulations taking into account the coupling between flow aggressiveness and material characteristics have to be made. In previous works ([Fortes-Patella, 1998a], [Fortes-Patella, 1998b], [Fortes-Patella, 2001]), a physical scenario and a numerical approach have been proposed to model and to analyse the cavitation erosion phenomena.

The physical scenario considers that the cavitation erosion is caused by the impacts of pressure waves emitted during the collapse of vapour structures. These pressure waves generate pits when they hit the target. The numerical approach, applied to study the incubation period of cavitation damage, is based on an energy balance between vapour structures, pressure waves and the solid material.

Thanks to previous simulations, the characteristics of the pressure waves responsible for the generation of an isolated pit can be determined from the geometric characteristics of the pit. After measuring the depths on a target previously mirror-polished and then exposed to a cavitating flow during incubation period, a software developed in our team locates the pits, evaluates their geometric characteristics, and calculates the properties of the pressure waves [Fortes, 2000].

An accurate estimation of the pressure wave characteristics requires the pits to be isolated (or at least not too many of them being superposed). Pitting tests must be short enough to avoid too many overlapping, but long enough to get a good statistic population of the impacts endured by the material.

After getting a statistic population of pressure waves emitted by the cavitating flow and damaging the target, simulations can be done to evaluate the mass loss through time. This requires to calculate how the material evolves when it is impacted, and how the mass loss occurs. In this way, a software was developed to simulate the generation of cavitation impacts on a solid surface. From a pitting test concerning a material, a given cavitation condition and a test duration, the software predicts the damage of the material exposed during different durations to the same cavitating flow. Two approaches of the mass loss have been implemented in the software.

The first one is based on the phenomenological model proposed by [Karimi, 1987]. This model is one-dimensional. The work-hardening of the material is taken into account. When a pressure wave impacts the material, a plastic deformation energy is absorbed per surface unit, resulting in the deformation of the surface of the target, and the work-hardening of the material under the point impacted. As time goes, plenty pressure waves impact the same point, thus increasing both the deformation of the surface and the work-hardening of the material, until the material cannot absorb more energy without breaking at that point. It means that, from the moment when the material has absorbed a certain energy quantity, every new incoming of energy through pressure waves will lead to the erosion of the material. Two ways of calculating the

mass loss have been implemented from this model, and will be presented, compared and discussed.

The other way of calculating the mass loss is based on the model proposed by [Reboud, 2001], who considers that the erosion is caused by the fatigue of the material subjected to pressure cycles. The repartition of deformation energy in the material can be calculated from the characteristics of the pressure wave impacting the surface. The energy thus remaining in the material after the impact can be linked to a number of cycles before rupture occurs. This number of cycles corresponds to a damage increment of the material. As time goes, new impacts bring energy to the material, and thus the damage increases in the material. When a point reaches a damage criteria, the material breaks at this point, in the bulk of the material. This model will be presented, compared to the previous model, and discussed.

NOMENCLATURE

a	removed layer following the extrapolation of the material properties beyond rupture assumption in Karimi & Leo's model	(m)
a'	removed layer following the saturation of the material properties beyond rupture assumption in Karimi & Leo's model	(m)
C	coefficient of the fatigue energy criterion	(J/m^3)
e_{int}	internal efforts energy density	(J/m^3)
h_1	depth before overlapping of pits for a material which didn't endure rupture in Karimi & Leo's model	(m)
h_2	depth resulting from the overlapping of pits in Karimi & Leo's model	(m)
h_c	deformed depth for a fully work-hardened material	(m)
h_i	depth engendered by an impact on a virgin surface in Karimi & Leo's model	(m)
n	work-hardening coefficient	(-)
D	damage function in Reboud's model	(-)
E_{pl}	residual plastic energy	(J)
E_{wave}^{mat}	impacting wave energy	(J)
H	maximum depth of a pit	(m)
K	stress-strain curve coefficient	(Pa)
L	maximum work-hardened depth	(m)
N_r	number of cycles to rupture under cyclic solicitation	(-)
$R_{10\%}$	radius of a pit a 10% of its maximum depth	(m)
V_{pit}	volume of a pit	(m^3)
$\beta = \frac{E_{wave}^{mat}}{V_{pit}}$		(J/m^3)
δ	exponent of the fatigue energy criterion	(-)
$\gamma_{n/1}$	ratio between the energy increment after n impacts and after the first impact in Reboud's model	(-)
$\eta = \frac{E_{pl}}{E_{wave}^{mat}}$		(-)
θ	shape coefficient	(-)
σ_e	elastic limit	(Pa)
σ_r	rupture limit	(Pa)

1. SCOPE AND TOOLS

Following numerical studies made by [Fortes, 1994, 1998], which enabled to study the shape of the pits resulting from microjet and pressure waves loadings, the pressure wave has been assessed to be the mechanism responsible for the erosion of materials exposed to cavitating flows. It enabled to propose the following scenario, summered on figure 1:

- the vapour cavity has an erosive potential power P_{pot}
- only a fraction of the bubbles present in the cavity can eventually affect the solid boundary. They represent the erosive potential power $\mathcal{P}_{pot}^{mat}$ that can be seen by the material. The ratio between P_{pot} and $\mathcal{P}_{pot}^{mat}$ is η^{**}
- following the assumption that pressure waves are responsible for the erosion, we consider that a fraction η^{*} of $\mathcal{P}_{pot}^{mat}$ finally damages the material. This power is $\mathcal{P}_{waves}^{mat}$, and corresponds to an energy E_{waves}^{mat}
- a pressure wave impacting the solid boundary deforms it plastically. The residual plastic energy E_{pl} is a fraction η of E_{waves}^{mat}
- if the material is impacted for the first time by the pressure wave (that means there is no pits overlapping), the volume V_{pit} of the pit is proportional to E_{pl}: $E_{pl}=\alpha V_{pit}$ where α is a property of the material. We can also write:

$$E_{wave}^{mat} = \frac{\alpha}{\eta} V_{pit} = \beta V_{pit}$$

Parameter β can be calculated by numerical simulations, and seems constant for a given material.

This article aims at showing how erosion models have been implemented in this scenario.

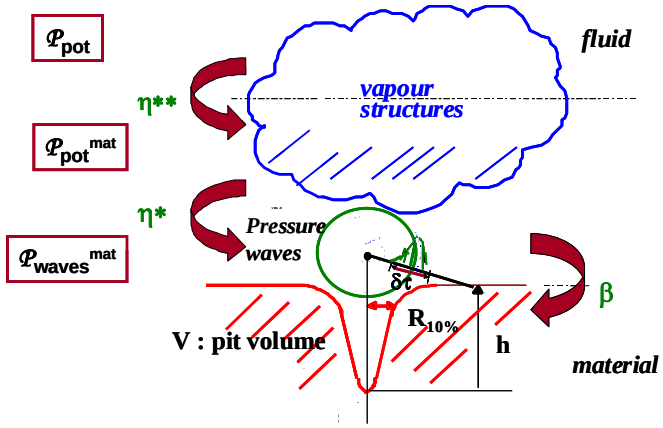

Figure 1: *summary of the cavitation erosion scenario proposed*

The cavitation erosion process is divided into three steps (see figure 2):

- the incubation period, during which the material only sustains elasto-plastic deformation, without mass loss

- the acceleration period, during which the mass loss begins
- the steady-state erosion period, during which the mass loss rate is constant.

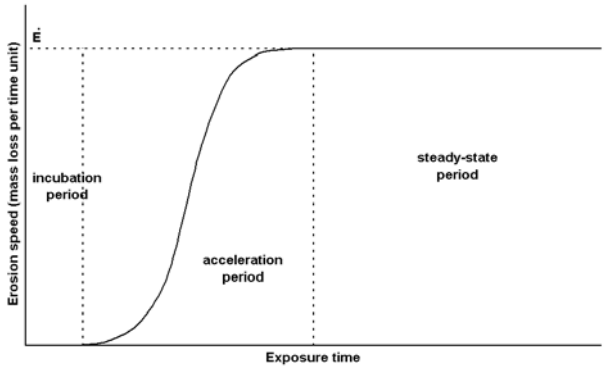

Figure 2: *the different periods of the cavitation erosion process [Karimi, 1987]*

This typical curve enables to define the steady-state erosion speed $\dot{E}$, which is the mass loss per time unit during the steady-state period.

As we will see below, models proposed by [Karimi, 1987] and [Reboud, 2001], intended to predict the erosion of a material exposed to a cavitating flow, require data that can be obtained from pitting tests. This is the case of the models that will be presented in this article. These tests are made during the incubation period. Their aim is to furnish the geometrical characteristics of the pits generated by the cavitation aggressiveness in order to deduce the characteristics of the pressure loadings endured by the solid, and thus, to evaluate the flow aggressiveness. The idea to use the material as a captor was proposed by [Knapp, 1955] because of the difficulty to get precise information from other captors: the time scale, of the order of 10 ns, is too short to enable proper answer of the captor; the space resolution is also problematic, because the surface of the captor must be smaller than the dimension of the impact in order not to underestimate it by averaging the pressure pulse on the whole surface of the captor. Pitting tests are today widely used to process erosion prediction ([Karimi, 1987], [Berchiche, 2001], [Dular, 2004]…). However, their reliability has never been studied.

Pitting tests have to respect few criterions to be pertinent:

- they must provide enough pits to furnish a population characteristic of what is endured by the material
- there must not be too many pits so that they do not overlap, which would lead to difficulties to measure their characteristics, and consequently would prevaricate the flow aggressiveness evaluation
- the initial surface must be mirror-polished to enable the geometrical characteristics of the pits to be measured accurately
- the initial level of the sample must be determined as accurately as possible so that the radius, depth and volume of the pits are correctly measured, which requires both a good initial surface state and not too many pits.

Consequently, a compromise has to be found concerning the time exposure of the sample to the cavitating flow, in order to get enough pits to be pertinent, but not too many which may lead to a lack of information.

Tools have to be used to get information from the pitting test. An example of method to evaluate the flow aggressiveness from a pitting test is given in [Fortes, 2000]. The first step consists in measuring the depth all over the pitted surface. This can be done for example by using 3D laser profilometry (see [Fortes, 2000]) or rugosimetry. The second step consists in analysing the measures to detect and characterize the pits. This is done thanks to a software, ADRESSE, which treats and analyses pitting tests to evaluate the radius and maximum depth of the pits. These characteristics enable to evaluate the properties of the pressure wave responsible for the formation of each pit thanks to these geometrical data combined with numerical simulations (see [Fortes, 1994, 1998]). After analysing the sample depths, ADRESSE furnishes a list of the pits radius, depth, volume, and evaluates the energy and pressure amplitude of the pressure wave that engendered them, and the distance between the solid boundary and the emission location of the pressure wave. Some of this data will be used as entries of the erosion models.

2. CAVITATION EROSION MODELS

The first works made in order to predict cavitation erosion tried to establish a correlation between one or more mechanical properties of the materials (such as their yield strength or hardness) and their erosion through time. Although the results were correct in the specific conditions in which they were obtained, they didn't prove their efficiency when used in different conditions. Such methods and discussions about these approaches can be found in [Thiruvengadam, 1964], [Lichtman, 1964], [Hamitt, 1970], [Heymann, 1970], [Kato, 1975], [Hammitt, 1979], [Kato, 1983], [Rao, 1984], [Heathcock, 1982], [Ball, 1983], [Hattori, 2004].

It can be explained by considering the complexity of the cavitation erosion phenomenon, in which hydrodynamical, mechanical, metallurgical and chemical behaviours interact. Consequently, scenarios taking into account these phenomenon and their interactions have to be developed in order to accurately predict the erosion of a material exposed to a cavitating flow through time.

This is the aim of the cavitation erosion models. They follow a 4 steps strategy:

- pitting tests: as explained in the previous paragraph, they have to be done properly in order to get a reliable pits population. In the one hand, they must provide enough indentations to enable to deduce the different loadings endured by the material. On the other hand, there must not be too many pits to avoid their overlapping, which would lead to difficulties to precisely determine their geometric characteristics

- measurements of the geometric characteristics of the pits

- evaluation of the erosive aggressiveness: following the proposed scenario concerning the cavitation erosion mechanisms, the characteristics of the pits enable to estimate the pressure loadings applied on the material

- simulation through time: by simulating the repetition through time of the pressure loadings endured by the material, it is possible to evaluate the material mass loss through time.

Two cavitation erosion models are presented below. In the present paper, we focus on the evaluation of the flow aggressiveness and the mass loss simulation through time, the other points being treated elsewhere (see for example [Fortes, 2000]).

2.1. Karimi & Leo's phenomenological model

This model has been presented in details in [Karimi, 1987]. It is based on the assumption that pressure loadings progressively lead to the work-hardening of the material, until it cannot sustain any energy supply and thus breaks.

2.1.1. Assessed material behaviour

Work-hardening is a very common behaviour of materials. Metals have a crystal structure, which means that their atoms occupy specific positions forming what is called a mesh, and that this mesh is repeated through the solid. However, crystals are not perfect, and there exist defaults in the structure: atoms are sometimes missing where they should be, which leads to the reorganization of the surrounding atoms. These defaults are called dislocations. When a metal endures a stress superior to its elastic limit, dislocations propagate, and they can interact: a dislocation prevents an other dislocation from moving. Consequently, a superior stress is necessary for the flow to go on. As the metal endures such stresses, more and more dislocations interact, thus leading to the hardening of the metal, known as "work-hardening". This phenomenon is illustrated by the stress-strain curves $\sigma = \sigma_e + K\varepsilon^n$ (see figure 3).

Let us consider a mono-dimensional situation, in which a metal endures a stress at its surface. When the stress ceases, residual deformations remain in the layer that has been work-hardened. If "x" is the depth perpendicular to the surface, "l" the depth of the work-hardened layer (this means that for $x<l$, the metal is work-hardened and presents a residual deformation, and for $x>l$, the metal is not work-hardened and doesn't present a residual deformation), and ε_s the residual deformation at the surface (we suppose that no rupture happened, which means $\varepsilon_s<\varepsilon_r$), the residual deformation at the depth x is given by:

$$\varepsilon(x) = \varepsilon_s\left(1-\frac{x}{l}\right)^{\theta}$$

This relation is known as the work-hardening profile of the metal (see figure 3).

If we now consider that the stress applied to the metal leads to its rupture, the residual surface deformation is ε_r, and the metal is work-hardened over a layer of maximum width, denoted L. The work-hardening profile of the material is then given by the relation:

$$\varepsilon(x) = \varepsilon_r\left(1-\frac{x}{L}\right)^{\theta}$$

with the origin of the x axis taken at the free surface of the metal. While the metal breaks and the free surface evolves, this profile is simply translated. The maximum width of work-hardening L and the shape coefficient θ are properties of the metal. These parameters can be determined thanks to micro/nano-indentation measurements (see [Berchiche, 2000]).

Following a mono-dimensional hypothesis, the stress and strain state of the metal can be deduced by determining the residual surface deformation, and then using the work-hardening profile and the stress-strain relation: the work-hardening profile allows to calculate the deformation in the metal in function of the width, and the stress-strain relation enables to deduce the residual stress in the metal thanks to the residual deformation (see figure 3).

In this model, it is assumed that the metal absorbs energy when impacted, which leads to its progressive work-hardening, until the maximum work-hardening profile is reached. From then, any new energy income will lead to the metal rupture, leaving the remaining metal in a maximum work-hardening situation (see figure 4).

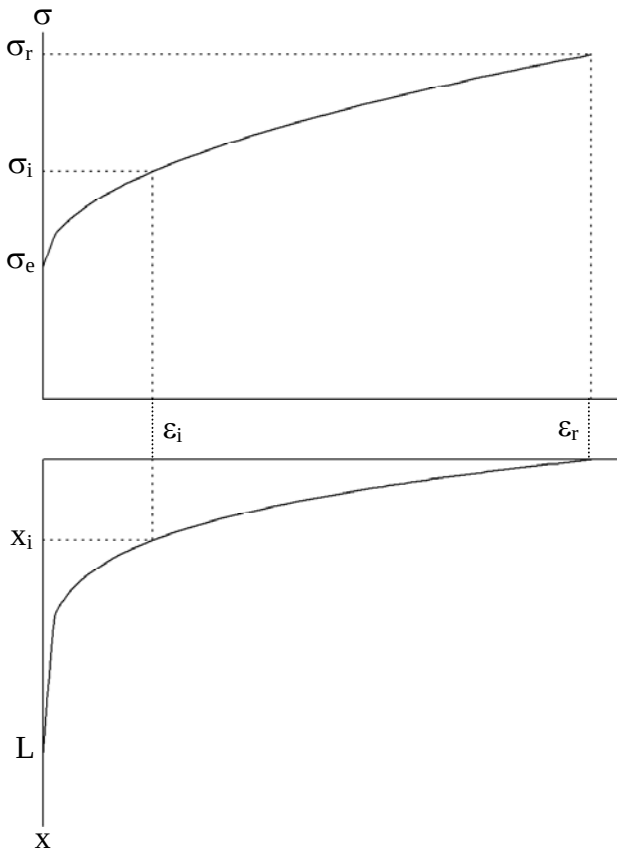

Figure 3: *case of a metal that endured rupture: its residual surface deformation is ε_r, and it is work-hardened over L width. At the width x_i from the free surface, the residual deformation is ε_i, and it corresponds to a residual stress σ_i.*

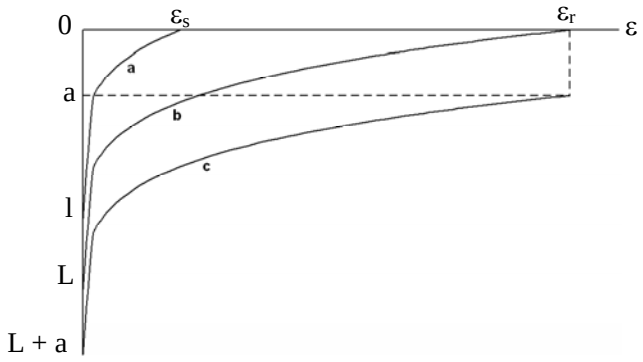

Figure 4: *curve a): after an impact, the metal is partially work-hardened over a "l" width, with a residual surface deformation ε_s; curve b): after plenty impacts overlapped at the same point, the material reached its maximum work-hardening profile, corresponding to a L work-hardened width, with a residual surface deformation ε_r; curve c): a new impact at this point led to the rupture of the metal over an "a" width, the remaining metal presents a maximum work-hardening profile that has been translated.*

2.1.2. Calculation code

A calculation code has been developed to use this model. The sample is represented by a 2D table, in which the value of each cell corresponds to the depth at this point.

We have seen at the first paragraph that the depths measured on the sample damaged by a pitting test during a given exposure time are analysed by ADRESSE software, which provides a list of the indentations characteristics. Amongst those characteristics are the maximum depth H of the indentation and its radius $R_{10\%}$ measured at a depth H/10 (see figure 5). These two characteristics are used as entries in the model.

The calculation code chooses one indentation after an other in the list, and randomly places it on the sample. Numerical studies (see [Fortes, 1998]) showed that the profile of an indentation engendered by a pressure wave on a virgin surface (that means that the surface has not been impacted before) is axisymetric and follows a polynomial profile adimensionalised by its H and $R_{10\%}$ characteristics:

$$\frac{h}{H} = \sum_i \alpha_i \left(\frac{r}{R_{10\%}}\right)^i$$

where h is the local deformed depth, and r the local radius within the indentation (see figure 5). This is the shape of the indentations to be simulated on our calculation code. For each point of the sample situated in the indentation, the depth is simply calculated following this profile if the elementary surface concerned is virgin.

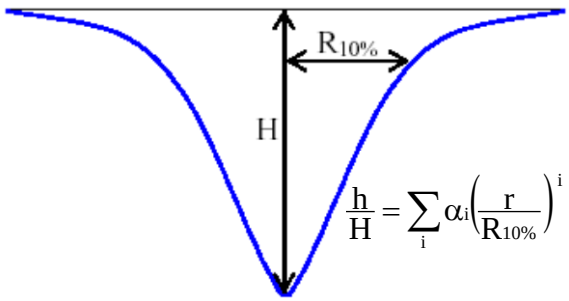

Figure 5: *the profile of an indentation engendered by a pressure wave on a virgin surface is assessed to follow a polynomial relation, adimensionalised by its maximum depth H and its radius $R_{10\%}$ at a H/10 depth*

As time goes and more indentations are simulated, the probability of overlapping increases. When an indentation has to be simulated on a work-hardened surface, calculation has to be made to deduce the resulting local depth on an elementary surface represented by a cell of the sample simulated. Karimi & Leo's model is mono-dimensional: consequently, the calculation will only take into account the local depth before overlapping and the local depth that would have resulted from the incoming indentation if the material had been virgin.

We will see how the problem of overlapping indentations leading to no material rupture is tackled. Let

us consider a cell of the table representing the sample: this cell corresponds to an elementary surface. This point has been impacted yet, consequently its depth h_1 is not 0. The local free surface has been deformed because the material absorbed plastic deformation energy W_1 on the elementary surface. This energy can be linked to the engendered depth by the relation:

$$W_1 = \sigma_e h_1 + \frac{B}{A} h_1^A$$

$$\text{with} \begin{cases} A = \dfrac{n\theta + \theta + 1}{\theta + 1} \\ B = \dfrac{K\varepsilon_r^{\frac{n}{\theta+1}}}{n+1} \left(\dfrac{\theta+1}{L} \right)^{\frac{n\theta}{\theta+1}} \end{cases}$$

Details of this calculation (and of the others to come) can be found in [Choffat, 2003, 2]. We see here that the stress-strain relation is an entry: this is a problem we meet because this relation is easy to get in a quasi-static situation, but not at the very high deformation speeds we are confronted with. The work-hardening profile of the material also needs to be determined: this can be done thanks to micro- or nano-indentation tests (see [Berchiche, 2000]), but this is not common and thus has to be done each time a new material is to be tested.

If the surface had been virgin, the new impact would have engendered a h_i depth at the point considered. That means that the elementary surface there would have absorbed a plastic deformation energy W_i, linked to the h_i depth by the relation:

$$W_i = \sigma_e h_i + \frac{B}{A} h_i^A$$

We assume that all the energy brought to the elementary surface remains in the material. Consequently, the total plastic deformation energy W_2 absorbed by the elementary surface is $W_2 = W_1 + W_i$. This total energy is linked to a h_2 depth by a relation of the same shape:

$$W_2 = \sigma_e h_2 + \frac{B}{A} h_2^A$$

Thus, we get a relation between the local depth before overlapping h_1, local depth that would have been engendered on a virgin surface by the new indentation h_i, and local resulting depth h_2:

$$\sigma_e h_2 + \frac{B}{A} h_2^A = \sigma_e \left(h_1 + h_i \right) + \frac{B}{A} \left(h_1^A + h_i^A \right)$$

Here is how the evolution of the material deformation during incubation period is dealt with in our calculation code. This can last until the total plastic deformation energy absorbed by the elementary surface reaches a critical value W_c, corresponding to a h_c depth, representing a fully work-hardened material at this point. When the total energy is superior to this value, the material cannot sustain the new energy income because it cannot work-harden anymore, and thus it breaks. The question of the material behaviour in this situation has then to be tackled.

a) Rupture criterion: first approach

Karimi & Leo suppose that the mechanical properties of the material can be extrapolated beyond rupture following the same relation than before rupture (see figure 6).

With this hypothesis, if we consider a fully work-hardened elementary surface that has to absorb a W_i energy, the relation between the local depth h_c before the new impact, the local depth h_i that would have been generated by the new impact, and the resulting local depth h_2 is the same than during incubation period:

$$\sigma_e h_2 + \frac{B}{A} h_2^A = \sigma_e \left(h_c + h_i \right) + \frac{B}{A} \left(h_c^A + h_i^A \right)$$

The removed layer "a" is then simply given by the difference $a = h_2 - h_c$.

If the material has endured rupture before the new impact, the local depth h_1 is superior to h_c:

$$h_1 = h_c + a_1$$

where a_1 is the eroded layer before the new impact.

The work-hardening profile of the remaining material is the full work-hardened material one, translated of a_1 depth. Relation:

$$\sigma_e h_2 + \frac{B}{A} h_2^A = \sigma_e \left(h_c + h_i \right) + \frac{B}{A} \left(h_c^A + h_i^A \right)$$

thus provides the increase a_2 of the eroded layer:
$a_2 = h_2 - h_c$.

The total eroded layer is then $a = a_1 + a_2$.

b) Rupture criterion: second approach

An other hypothesis can be done concerning the material behaviour: we can suppose that the mechanical properties reach a saturation state when the material breaks (see figure 6). This hypothesis seems more reliable than the previous one.

Following this hypothesis, the increment of eroded layer removed by a new impact from a fully work-hardened material is given by relation:

$$a' = \frac{\sigma_e h_i + \dfrac{B}{A} h_i^A}{\sigma_e \varepsilon_r + \dfrac{K\varepsilon_r^{n+1}}{n+1}}$$

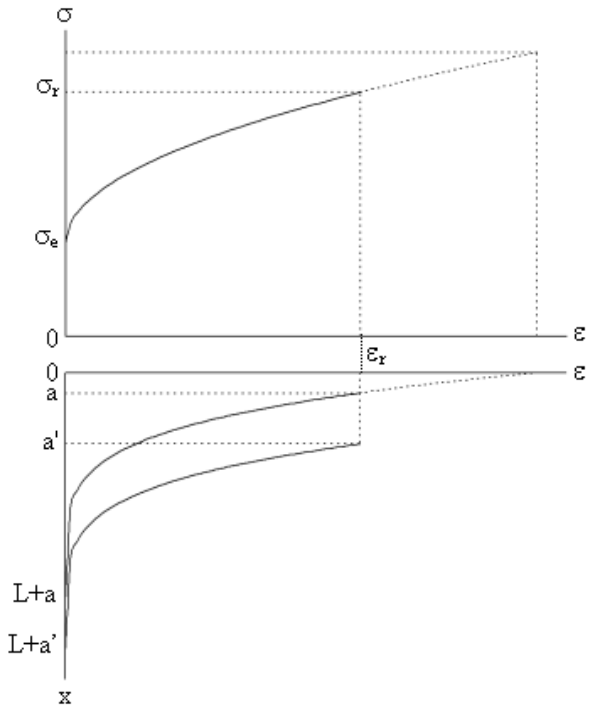

Figure 6: *difference between the two rupture criterion in Karimi & Leo's model. Following the first approach, the stress-strain curve and the work-hardening profile can be extrapolated beyond rupture; following the second approach, these mechanical properties reach saturation at rupture. For a same energy income, the removed layer is not the same following these two criterions*

The two rupture hypotheses have been implemented in our calculation code.

2.2. Reboud's fatigue model

A more complete model has been proposed by [Reboud, 2001]. It takes into account work-hardening and fatigue phenomena. Considering that cavitation erosion occurs after repeated pressure loadings on the metal, this model considers that the mechanism responsible for metal rupture is fatigue.

2.2.1. Assessed material behaviour

As we have seen in the previous paragraph, rupture happens when a material is solicited beyond its rupture limit. However, metals can break if they endure cyclic solicitations, even though these solicitations remain under the rupture limit of the material or even its elastic limit. This is due to the progressive propagation of microcracks on the metal at each solicitation cycle. This phenomenon is referred to as fatigue. When the material is solicited between its elastic limit and its rupture limit, the process is called oligocyclic fatigue, because the material sustains global plastification at each cycle, which leads to its rupture after few cycles. The rupture of a metal solicited in fatigue happens after a given number N_r of solicitation cycles which depends on the intensity $\Delta\sigma$ of the solicitation. This relation is illustrated by the Wöhler curve. An example of the Wöhler curve concerning steel is given in figure 7.

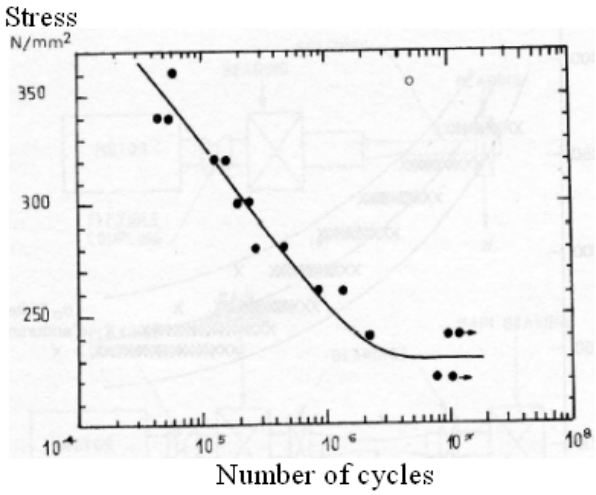

Figure 7: *Wöhler curve indicates the number of cycles after which the metal breaks under a given cyclic solicitation [Lemaignan, 2003]*

Taking into account microcracks propagation require microstructural information and demanding calculations. This would be too complex and long, so Reboud's model relies on a simplified approach within the hypotheses of continuum mechanics. At each solicitation cycle, the material is supposed to be solicited over a given volume. The solicitation is not the same everywhere in the volume. Each point of the volume is supposed to sustain a particular solicitation increment, which we call ΔX for the moment. This increment can be expressed in terms of stress, strain, or energy. It is linked to the notion of damage. Behind this notion is the idea that the material evolves as it is solicited, and that its capacity not to break decreases as it endures more solicitations, until it cannot resist anymore and eventually breaks when it is too much damaged. Let us call D the function representing the damage of the material. In a general way, the material damage is supposed to be $D = 0$ when it is intact, and the material is supposed to break when its damage reaches the value $D = 1$. Between these two limits, the material endures a damage increment ΔD at each solicitation cycle.

The damage increment ΔD is linked to the solicitation increment ΔX. Different relations can be proposed depending on the situation considered. The criterion adopted in Reboud's model is the energy criterion proposed by [Ellyin, 1988]. When a material endures cyclic solicitation, its stress-strain curve follows a cyclic; in the case of oligocyclic fatigue where global plastification occurs, the material becomes smoother or harder until it reaches a steady behaviour (see figure 8). Integral calculation enables to deduce the energy increment Δe_{int} absorbed by the material at each cycle. After a given number N_r of cycles, the material breaks. N_r is the number of cycles the material can endure before breaking when it absorbs an energy increment Δe_{int} at each cycle. In oligocyclic fatigue, which is the case in

cavitation erosion where pressure impulses can reach several GPa, N_r and Δe_{int} are linked by a relation [Ellyin, 1988]:

$$\Delta e_{int} = \frac{C}{N_r^{\delta}}$$

Parameters C and δ are characteristic of the material. They require plenty complex fatigue tests, and are thus very difficult to obtain. This is something we really lack, because, at the present time, we only know these parameters for stainless steel in the case of quasi-static tests. From results presented in [Lemaître, 1988], Reboud deduced:

$$C = 1.85\ 10^9\ J/m^3 \text{ and } \delta = 0.67$$

for 316L stainless steel.

This criterion allows to express the solicitation increment in terms of energy, and is linked to the number of cycles before rupture.

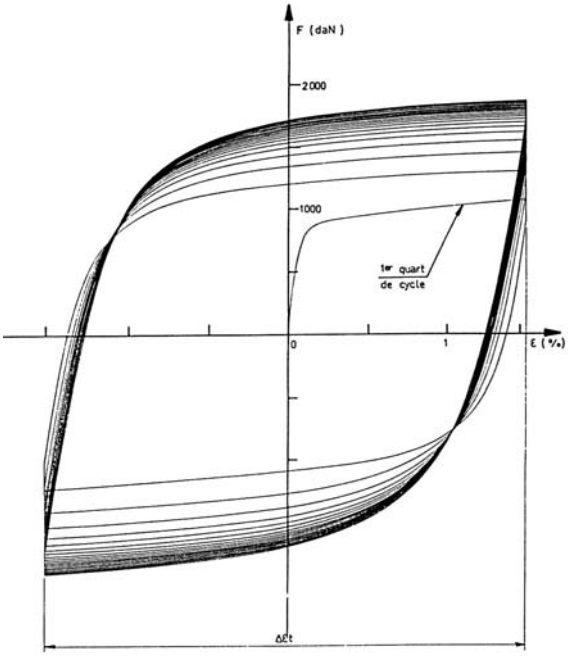

Figure 4.4. *Exemple de cycles effort-déformation. Consolidation cyclique: Acier Z2 CND 17 12 (acier AISI 316L) à 20°C*

Figure 8: *cyclic consolidation of 316L stainless steel [Bathias, 1997]*

The damage increment ΔD and its accumulation still remain to be defined. For this, we consider a simple situation: a material enduring constant cyclic solicitation, leading to its rupture after N_r cycles. If we suppose that each cycle evenly damages the material and that these damage increments can be added, we get the following relation at rupture: $N_r \times \Delta D = 1$. Consequently, the damage increment could be simply defined by

$$\Delta D = \frac{1}{N_r}$$

This definition is generalised to the case of solicitations of different amplitude: if the material endures a solicitation that would lead to its rupture after N_i cycles, the damage increment is

$$\Delta D = \frac{1}{N_i}.$$

The cumulative damage is

$$D = \sum_i \frac{1}{N_i}.$$

When this value exceeds 1, the material breaks. This is called the Palmgreen-Miner rule. It is important to note that this rule was not completely validated, but no better rule exists: fatigue phenomenon is extremely complex, and is influenced by microstructural aspects which cannot be known (defaults, phase changes, joint boundaries…), and is thus characterized by its huge randomness.

2.2.2. Calculation code

A calculation code has been developed to use this model. The sample is represented by a 3D table, in which the value of each cell corresponds to the cumulative damage at this point.

We have seen that the previous model requires geometric data from ADRESSE pitting test analysis. It's the same for this model, in which the volume V_{pit} and the radius $R_{10\%}$ of the indentations are used as entries. The calculation code chooses one indentation after an other in the pit list, and randomly places it on the sample. The repartition of the damage engendered by this impact then has to be calculated.

Reboud developed, by a finite elements approach, a 2D axisymetric software that simulates the dynamic impact response of an elastoplastic medium subjected to a spherical pressure wave impact (see [Reboud, 1987] and [Fortes, 1998]). The code provides the complete transient evolution of the material (strain, stress and energy fields) and the permanent surface deformations (the pit profiles). Moreover, it enables to calculate, the internal efforts energy density per volume unit remaining in a solid after a transient pressure impingement (Figure 9).

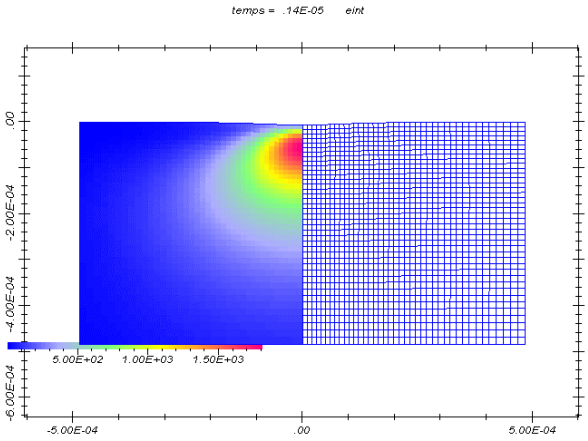

Figure 9 : *internal efforts energy density e_{int} after the impact of a pressure wave. Pressure wave characteristics: maximum amplitude P = 1.5 GPa, emission distance from the boundary L = 0.1mm, passage time at half-amplitude (to be defined later) δt = 0.5 µs. Material properties: σ_e = 260 MPa, σ_r = 390 MPa, ε_r = 3.5% [Reboud, 2001]*

Making use of this simulation code, numerical tests have been carried on by [Reboud, 1987] and [Faure, 2000] to calculate the evolution of the internal efforts energy repartition in the case of repeated impacts of same characteristics and axis. It has been found that the shape of this repartition is close to the shape of the energy repartition after one impact. Repeated impacts of same axis but different characteristics have also been simulated: it has been found a difference in the shape of the energy repartition, but not too significant.

It is important to note that impacts of different axis have not been simulated: they should probably lead to a difference in the shape of the energy repartition. Consequently, we consider, for the moment, that the energy repartition is the same whatever the situation is, and corresponds to that of identical repeated impacts of same axis. The simplified expression of this repartition is:

$$\Delta e_{int}(r,z) = \Delta e_{int}^{max} g_r(r, R_{10\%}, L')g_z(z, R_{10\%}, L')$$

where r is the radial position, z the depth, and g a function close to a gauss function.

Parameter L' is defined by :

$$L' = L\left(\frac{C_{liq}\delta t}{L}\right)^{\frac{1}{3}},$$

where L is the distance between the solid boundary and the emission location of the pressure wave, C_{liq} the propagation celerity of the wave in the liquid, and δt the passage time of the wave at the half of its amplitude (see figure 10).

In the present study, based on previous works (Fortes, 1998), we consider: L=L(R10%)≈ R10%/3. We adopt also the value $\frac{C_{liq}\delta t}{L} = 1$. Further works are required to analyse the influence of these values on damage prediction.

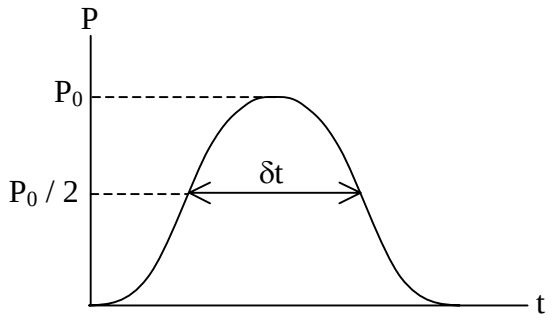

Figure 10: *when the pressure wave propagates, the pressure in the fluid increases, reaches a maximum P_0, and then decreases. δt is the duration between the pressure reaches $P_0/2$ while increasing and $P_0/2$ while decreasing*

The damaged zone concerns a r_{max} = 4L' distance around the impact axis, and a z_{max} = 3L' distance from the surface. The maximum damage Δe_{int}^{max} is reached at a L'/3 distance from the surface on the axis of the impact. Figures 11 and 12 show the energy repartition used in our calculation code following results obtained by [Reboud, 2001].

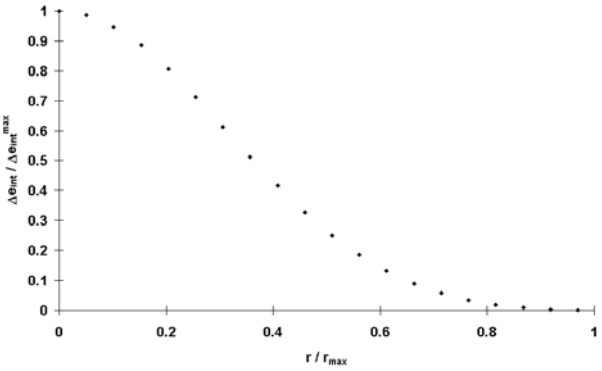

Figure 11: *no-dimensional repartition of the internal efforts energy density used in our calculation code in the radial direction*

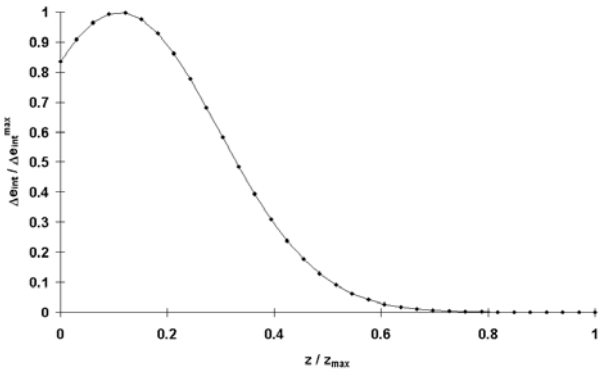

Figure 12: *no-dimensional repartition of the internal efforts energy density used in our calculation code in the depth direction*

According to simulations performed by [Reboud, 2001], Δe_{int}^{max} is given by the relation:

$$\Delta e_{int}^{max} = \frac{\eta \gamma_{n/1} E_{wave}^{mat}}{10 L'^3}$$

Parameter L' has been defined previously. At the first paragraph, we explained that E_{mat}^{wave} is linked to the indentation volume by the relation $E_{wave}^{mat} = \beta V_{pit}$, where β can be calculated by numerical simulations and is constant for a given material [Fortes, 2001], [Challier, 2002].

Parameter η has also been presented in paragraph 1: it corresponds to the ratio between the energy deforming plastically the material and the energy of the pressure wave seen by the boundary. This parameter depends on the amplitude of the pressure wave [Fortes, 1998b], [Challier, 2002]. However, for simplification, a mean value is used in the model. Further studies will enable to evaluate the error introduced by this simplification.

Parameter $\gamma_{n/1}$ is defined by:

$$\gamma_{n/1} = \frac{\Delta e_{int}^{max}(n)}{\Delta e_{int}^{max}(1)}$$

where $\Delta e_{int}^{max}(1)$ is the maximum increment of the internal efforts energy density after the first impact, and $\Delta e_{int}^{max}(n)$ is the maximum increment of the internal efforts energy density after the n^{th} impact.

As we have seen previously, the shape of the energy repartition in the case of repeated impacts is the same as the shape of the energy repartition after one impact. However, the increment of energy is not the same: in the case of stainless steel, the energy increment decreases between the first impact and the others, to reach a constant value after few impacts (Figure 13).

In this first application of this model, the variation of this increment is not taken into account. Consequently, $\gamma_{n/1}$ is taken constant, equal to the ratio between the stabilised energy increment and the energy increment at the first impact (i.e., $\gamma_{n/1}$=50%) . This is how the internal efforts energy density per volume unit is evaluated in the calculation code, using pitting test results (volume and radius $R_{10\%}$ of the indentations).

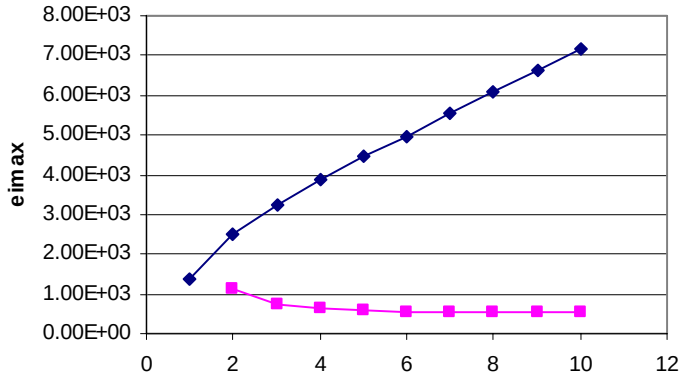

Figure 13: *evolution of the maximum internal efforts energy density after successive impacts (diamonds) on a stainless steel. The squares show the increment* Δe_{int}^{max} *between two successive impacts [Reboud 2001]*

When this increment has been calculated, the damage increment can be deduced thanks to Ellyin & Golos's energy criterion:

$$\delta D = \frac{1}{N_i} = \left(\frac{\Delta e_{int}}{C}\right)^{\frac{1}{\delta}}$$

The cumulative damage is then incremented:

$$D(i+1) = D(i) + \delta D$$

If it exceeds 1, rupture is supposed to happen. Following this assumption, the material layer situated between the surface and the point where rupture happened is removed. Therefore, energy distribution is simulated by an 2D axisymetrical approach, but rupture criterion is based on a mono-dimensional assumption.

3. COMPARISON BETWEEN THE MODELS

3.1. Pitting test data

A first application of both models was performed based on experimental results obtained by EDF in the EDF Modulab test loop ([Simoneau, 1997], [Fortes, 2000]). An aluminum sample was exposed during 10s to a water cavitating flow. Measurements performed by laser profilometer corresponding to a surface of 100 mm^2 were treated by ADRESSE software and pit distribution was determined (Figures 14, 15 and 16).

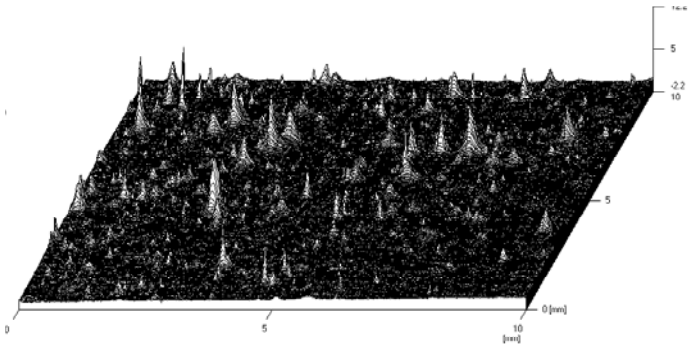

Figure 14: *visualization of the surface of an aluminum sample exposed to a cavitating flow during T=10s (water flow velocity=32m/s).*

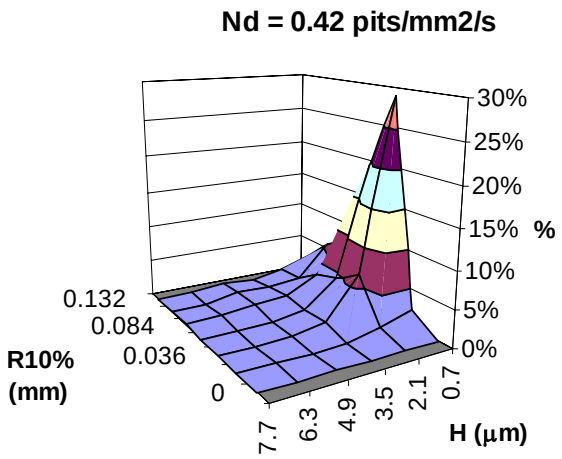

Figure 15: *the histogram illustrates the ratio between the number of pits for each class of depth "H" and radius "$R_{10\%}$". Aluminum sample; v=32m/s; water at 30°; T=10s*

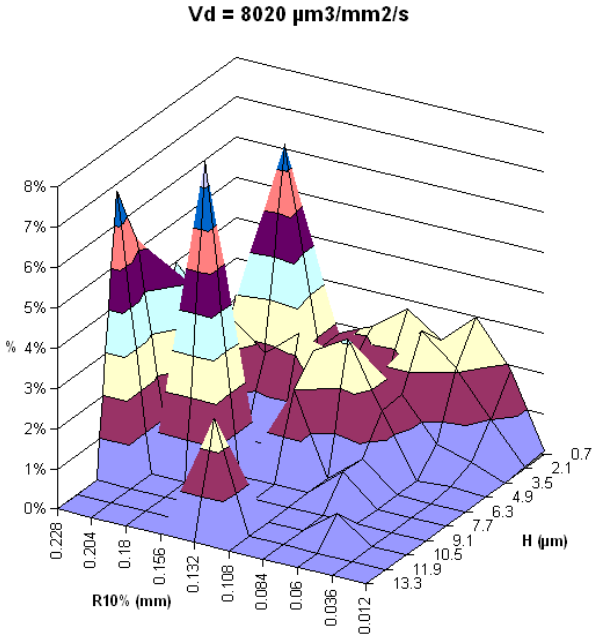

Figure 16: *the histogram illustrates the ratio between the global volume engendered for each class of depth "H" and radius "$R_{10\%}$".*

The indentations list obtained can then be simulated plenty times on a sample in order to estimate the mass loss through time.

3.2. Calculations conditions

For Karimi & Leo's model, the sample has been simulated by a 1000*1000 points surface corresponding to a 100 mm² surface (the step is thus 10 µm in both directions). The value at each point corresponds to the local depth.

For Reboud's model, the sample has been simulated by a 1000*1000*77 points volume corresponding to a 100 mm² surface and a 436µm depth; the step at the surface is 10 µm in both directions, and the step in depth is 5.66 µm. The value at each point corresponds to the local cumulative damage.

The method to mesh the depth of the sample in Reboud's model has to be explained. A mean value $\tilde{R}_{10\%}$ is calculated from all the radius $R_{10\%}$ level-headed by the volume of the indentation:

$$\tilde{R}_{10\%} = \frac{\sum_i \left(R_{10\%,i} V_i\right)}{\sum_i V_i}$$

As we have seen at paragraph 2.2.2, the maximum depth z_{max} damaged by a pressure wave emitted at a distance L from the boundary is given by $z_{max} = 3L$ (with the hypothesis $\frac{C_{liq}\delta t}{L} = 1$). In the present study, we have considered $R_{10\%} \approx 3L$. Consequently, $z_{max} \approx R_{10\%}$. We can thus calculate the maximum damaged depth $\tilde{z}_{max}$ of a pit which radius $R_{10\%}$ is $\tilde{R}_{10\%}$: $\tilde{z}_{max} \approx \tilde{R}_{10\%}$. When we study the repartition of the internal efforts energy density (see figure 12), we find that we must choose a step $\Delta z = 0.031\, z_{max}$ to take into account a maximum 10% variation of this energy between two points. This is what we want for the indentation which radius $R_{10\%}$ is $\tilde{R}_{10\%}$: the depth step is $\Delta z = 0.031\tilde{z}_{max} \approx 0.031\tilde{R}_{10\%}$. The indentations list also provides us with the maximum radius $R_{10\%,max}$, from which the maximum damaged depth $\overline{Z}_{max}$ of all the indentations can be deduced:

$$\overline{Z}_{max} \approx R_{10\%,max}.$$

The number of points N_z in the depth direction is then given by $N_z = \frac{\overline{Z}_{max}}{\Delta z} = 77$.

The 10% energy variation criterion has been chosen arbitrarily: consequently, further numerical tests are also required to test the influence of this criterion.

Concerning material characteristics, the following properties have been used for Karimi & Leo's model: σ_e=400MPa, σ_r=1020MPa, n=0.5, K=900MPa, L=200µm, θ=5, ρ=7900kg/m^3. They correspond to 316L stainless steel.

The following material properties have been used for Reboud's model: β=68J/mm^3, η=2%, $\gamma_{n/1}$=50%, C=1.85 10^9 J/m^3, δ=0.67, ρ=7900kg/m^3. These values also correspond to 316L stainless steel.

One of the big problems we face when trying to use the erosion models presented above is the lack of material data: the material properties (work-hardening profile in the one hand, energy criterion for fatigue damage in the other hand) are rarely used. Consequently, they are very difficult to find in literature, and specific tests should be done to get the required values. This explains why we have been obliged to use material properties for 316L stainless steel, even though the indentations simulated resulted from a pitting test made on an aluminium sample: pitting tests on aluminium are good quality ones, but we could only find material properties for 316L

stainless steel. This highlights our need to get mechanical data in order to validate the calculation codes.

3.3. Results

3.3.1. General remarks

Calculations have been made with the same indentations list for the two models. Results are displayed on figure 17 for Karimi & Leo's model ("saturation" corresponding to the hypothesis that material properties cannot be extrapolated beyond rupture, "extrapolation" corresponding to the hypothesis that material properties can be extrapolated beyond rupture) and 18 for Reboud's model: the results of these two models could not be displayed properly on the same figure because of the very different exposure times required to reach the erosion steady-state in the two models.

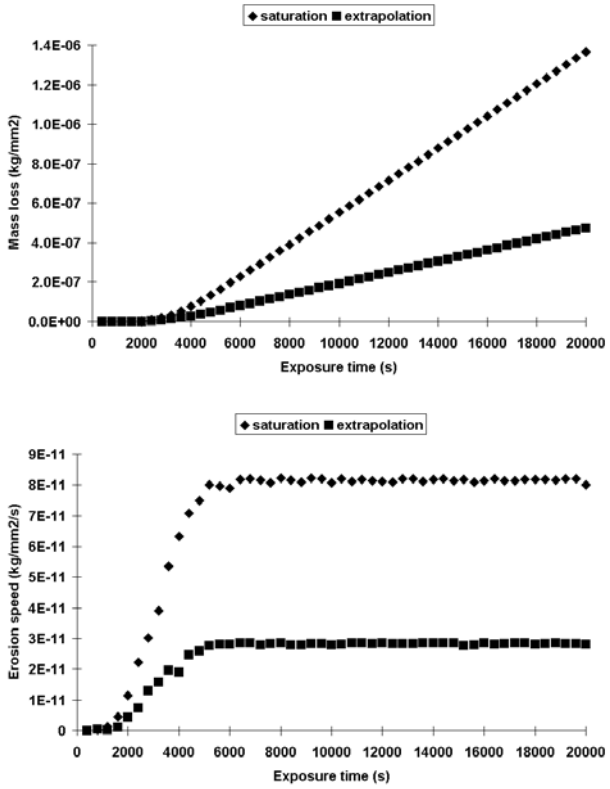

Figure 17: *mass loss (up) and erosion speed (down) calculated following the two rupture hypothesis of Karimi & Leo's model: "saturation" curves correspond to the hypothesis that the material properties cannot be extrapolated beyond rupture, whereas "extrapolation" curves correspond to the hypothesis that the material properties can be extrapolated beyond rupture*

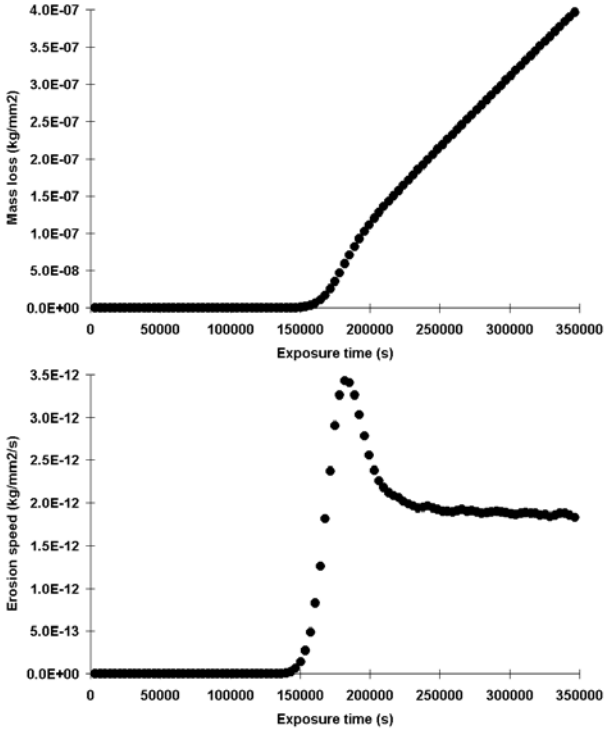

Figure 18: *mass loss (up) and erosion speed (down) calculated following Reboud's model*

Comments can be done about the curves presented in Figures 17 and 18:

- these curves enable to distinguish the incubation period, transient period, and steady-state period. For both Karimi & Leo's model rupture approaches, the transient period corresponds to an acceleration period: this is because the material progressively reaches full work-hardening all over the sample. For Reboud's model, the transient period begins by an acceleration period, and is followed by a deceleration period: this is because the biggest pieces of material are removed at the beginning of the rupture process (see [Fitch, 2002]). The same kind of curves can be found in [Steller, 2004].
- both approaches of rupture in Karimi & Leo's model lead to results of the same order for incubation time and erosion speed. When the material properties are extrapolated beyond rupture, the material is assumed to absorb more energy than when its material properties are assumed to reach saturation at rupture. It explains why the extrapolation hypothesis is less erosive than the saturation hypothesis.

3.3.2. Comparison to experimental values

It is interesting to compare the values predicted to experimental data. Mass loss tests have been performed on the MODULAB test rig by EdF (R&D) on aluminium samples with flow velocity 38 m/s [Simoneau, 1997]. The incubation time was found to be about 2h, after which the steady-state mass loss speed was about 0.022 mg/mm²/h. The list of indentations used for the calculations presented here was obtained on the same test rig, on an aluminium sample with flow velocity 32 m/s. Erosion aggressiveness increases with flow velocity (see for

example [Fortes, 2000]), consequently the simulations should lead to an underestimation of the mass loss because of the difference (even weak) between the flow velocities during the pitting test and the mass loss test. An other reason should lead to this expected underestimation: material properties used for our calculations correspond to stainless steel, which is more resistant than aluminium.

Before comparing calculations predictions to experimental data, it is important to define how the incubation period is evaluated: it corresponds to the abscissa of the intersection point between the tangent to the mass loss curve during steady-state period and the abscissa axis (see figure 19).

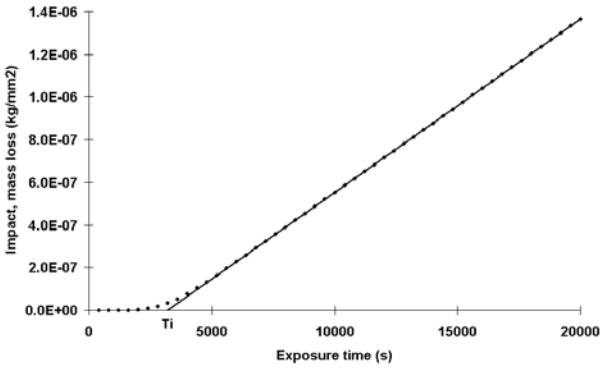

Figure 19: *we choose to define the incubation period as the moment when the tangent to the mass loss curve during the steady-state period crosses the abscissa axis. Here is shown the example for Karimi & Leo's model with the hypothesis that material properties reach saturation at rupture*

Concerning Karimi & Leo's model, contrarily to expected behaviour, the values predicted overestimate the experimental result: the saturation hypothesis at rupture leads to a predicted mass loss speed of 0.293 mg/mm²/h, and the extrapolation hypothesis at rupture to a predicted mass loss speed of 0.102 mg/mm²/h.

Concerning the incubation period, both rupture approaches of this model lead to a 1h incubation period, which is shorter than the experimental one. This unexpected result can be explained as follows: stainless steel cannot deform as much as aluminium because it is harder; consequently, it can be assessed that the deformed depth h_c (see paragraph 2.1.2) corresponding to a fully work-hardened layer will be bigger for aluminium than for stainless steel; indentations used from the pitting test made on aluminium have a depth quite close to the h_c depth of stainless steel; thus, the erosion of the material is predicted more quickly by using stainless steel data than it could be by using aluminium data.

Results provided by Reboud's model and considered physical parameters indicate a incubation period of about 37h. As expected, the mass loss speed predicted for a stainless steel sample is smaller than one measured for aluminium sample: the simulated value is about 0.0067 mg/mm²/h (to be compared with 0.022 mg/mm²/h in the case of measurements on aluminium).

Several tests are in progress in order to evaluate the influence of the mesh and to propose a mesh convergence criterion.

Other numerical tests have to be carried out in order to test the influence of the simulated surface and the considered parameters (for example, $\gamma_{n/1}$, $\frac{C_{liq}\delta t}{L}=1$, L=L(R10%)≈ R10%/3).

Further numerical tests are also need to test the influence of the material properties precision. Indeed, they are very difficult to determine for two reasons: first, they are rarely used; second, stress-strain relation and data required for the fatigue energy criterion are determined in quasi-static situations, whereas the cavitation erosion process is dynamic. This is an other lack we have to deal with.

CONCLUSION

Erosion models have been implemented in order to predict the mass loss thanks to data provided by pitting tests.

We will have to deal with some difficulties to validate our calculation codes: we lack material properties and experimental mass loss data enabling to validate our predictions.

Further tests remain to be done in order to test the influence of the precision of the simulated sample, and to test the influence of the precision of the material properties. This last point could highlight our need to get information about material behaviour to validate the models we use.

An other kind of tests will also be done, aiming at studying the need for good quality pitting tests, and the influence they can have on erosion prediction.

ACKNOWLEDGMENTS

The authors wish to express their gratitude to the Electricité de France (EdF – R&D) for its continuous support and for supplying experimental results. The authors wish also to express their gratitude to Jean-Luc Reboud for supplying scientific documents and numerical results. This research was supported by a doctoral grant from "Ministère de l'Education Nationale", France.

REFERENCES

[Ball, 1983] A. Ball, On the importance of work hardening in the design of wear-resistant materials, Wear, 91, 1983, 201-207

[Bathias, 1997] Bathias, Baïlon "La fatigue des matériaux et des structures", ed. Hermes, 1997.

[Berchiche, 2000] Berchiche N., Erosion de cavitation d'un métal ductile: étude expérimentale et modélisation, thèse soutenue le 17 octobre 2000 à Grenoble

[Berchiche, 2001] Berchiche, Franc, Michel, A cavitation erosion model for ductile materials, CAV2001

[Challier, 2002] Challier G., Mécanismes d'interactions fluide/structure et de transfert d'énergie en

érosion de cavitation, thèse soutenue le 20 décembre 2002 à Grenoble

[Choffat, 2003] Choffat T., Fortes-Patella R., Franc J.P., Archer A., A Procedure to account for overlapping in pitting tests, *Proceedings of CAV 2003 Symposium*, November 2003, Osaka.

[Choffat, 2003, 2] Choffat, Etude et modélisation de l'érosion de cavitation : influence de la durée d'exposition sur l'évaluation de l'agressivité érosive, DEA soutenu en septembre 2003 à Grenoble

[Dular, 2004] Dular, Bachert, Stoffel, Sirok, Relationship between cavitation structures and cavitation damage, Wear 257 (2004) 1176-1184.

[Ellyin, 1988] Ellyin & Golos, Multiaxial fatigue damage criterion, Journal of Engineering Materials and Technology 110 (1988) 63-68.

[Faure, 2000] Faure F., Modélisation de l'érosion de cavitation par calculs numériques, Master report, 2000.

[Fitch, 2002] Fitch, Tribolics Inc., Cavitation wear in hydraulic systems, Practicing oil analysis magazine, septembre 2002.

[Fortes, 1994] Fortes Patella, Analyse de l'érosion de cavitation par simulations numériques d'impacts, thèse soutenue le 25 février 1994 à l'Institut National Polytechnique de Grenoble.

[Fortes, 1998a] Fortes-Patella, R., and Reboud, JL., 1998, "A New Approach to Evaluate the Cavitation Erosion Power", Journal of Fluid Engineering , Transactions of the ASME, Vol. 120, June 1998.

[Fortes, 1998b] Fortes-Patella, R., and Reboud, JL.,1998, "Energetical Approach and Impact Efficiency in Cavitation Erosion", Proc. of 3rd International Symp. on Cavitation, Grenoble.

[Fortes, 2000] Fortes Patella, R., Reboud, JL., and Archer, A., 2000, "Cavitation Damage Measurements by 3D Laser Profilometry", Journal of WEAR, vol 246, pp. 59-67.

[Fortes, 2001] Fortes Patella, R., Challier, G., Reboud, JL., and Archer, A., 2001, "Cavitation erosion mechanism: numerical simulations of the interaction between pressure waves and solid boundaries", Proceedings of CAV 2001 Symposium, June 2001, Pasadena.

[Hammitt, 1970] F.G. Hammitt et al., A statistically verified model for correlating volume loss due to cavitation or liquid impingement. Characterization and determination of erosion resistance, ASTM, STP 474, American Society for Testing and Materials, Philadelphia, PA, 1970, 288-322

[Hammitt, 1979] Cavitation erosion : the state of the art and predicting capability, Applied Mechanics Reviews, volume 32, numéro 6, juin 1979

[Hattori, 2004] S. Hattori, R. Ishikura, Q. Zhang, Construction of database on cavitation erosion and analyses of carbon steel data, Wear 257 (2004), 1022-1029

[Heathcock, 1982] C.J. Heathcock et al., Cavitation erosion of stainless steels, Wear, 81, 1982, 311-327

[Heymann, 1970] F.J. Heymann, Toward quantitative predictionof liquid impact erosion. Characterisation and determination of erosion resistance, ASTM, STP 474, American Society for Testing and Materials, Philadelphia, PA, 1970, 212-248

[Karimi, 1987] Karimi, A., Leo, W.R., 1987, "Phenomenological model for cavitation erosion rate computation", Materials Science and Engineering 95, pp. 1-14.

[Kato, 1975] H. Kato, A consideration on scaling laws of cavitation erosion, International Shipbuilding Progress, vol. 22, n°253, 1975, 305-327

[Kato, 1983] Kato, Cavitation erosion in hydraulic machineries, IAHR monograph on cavitation, septembre 1983, Moscou

[Knapp, 1955] Recent Investigations of cavitation and cavitation damage, Trans. ASME 77

[Lemaignan, 2003] Lemaignan C., La rupture des matériaux, EDP Sciences, 2003

[Lemaitre, 1988] Lemaitre, Chaboche "Mécanique des matériaux solides", ed. Dunod, 1988.

[Lichtman, 1964] J.Z. Lichtman & E.R. Weingram, The use of a rotating disk apparatus in determining cavitation erosion resistance in materials, Proc. Symp. on Cavitation Research Facilities Technology, Ed. J.W. Holl & G.M. Wood, ASME, New York, 1964, 185-196

[Rao, 1984] P.V. Rao & H. Buckley, Predictive capability of long-terme cavitation and liquid impingement erosion models, Wear, 94, 1984, 259-274

[Reboud, 1987] Reboud, Réponse impulsionnelle d'un milieu élastoplastique : application à l'étude de l'érosion de cavitation, thèse soutenue le 29 septembre 1987 à l'Institut National Polytechnique de Grenoble

[Reboud, 2001] Reboud, JL., 2001, "Prévision de l'érosion de cavitation : couplage écoulement et matériau. Partie I : aspect matériau", Report - Commande EdF-R&D N°P41/C03332 – June 2001.

[Simoneau, 1997] Simoneau, Archer, Transposition of cavitation marks on different hardness metals, ASME Fluids Engineering Division Summer Meeting, June 1997

[Steller, 2004] Steller, Krella, Koronowicz, Janicki, Towards quantitative assessment of material resistance to cavitation erosion, Wear 258 (2005) 604-613

[Thiruvengadam, 1964] A. Thiruvengadam & H.S. Preseir, On testing materials for cavitation damage resistance, J. Ship. Res., 1964, 8, 39